Sensitivity estimations for cloud droplet formation in the vicinity of the high alpine research station Jungfraujoch (3580 m a.s.l.)

E. Hammer[1]**, N. Bukowiecki**[1]**, B. P. Luo**[3]**, U. Lohmann**[3]**, C. Marcolli**[3,4]**,**
E. Weingartner[1,*]**, U. Baltensperger**[1]**, and C. R. Hoyle**[1,2]

[1]Laboratory of Atmospheric Chemistry, Paul Scherrer Institute, 5232 Villigen PSI, Switzerland
[2]Swiss Federal Institute for Forest Snow and Landscape Research (WSL)-Institute for Snow and Avalanche Research (SLF), Davos, Switzerland
[3]Institute for Atmospheric and Climate Science, ETH Zurich, 8092 Zurich, Switzerland
[4]Marcolli Chemistry and Physics Consulting GmbH, 8092 Zurich, Switzerland
[*]now at: Institute for Aerosol and Sensor Technology, University of Applied Sciences and Arts Northwestern Switzerland, Switzerland

Correspondence to: C. R. Hoyle (christopher.hoyle@env.ethz.ch)

Abstract

Aerosol radiative forcing estimates suffer from large uncertainties as a result of insufficient understanding of aerosol–cloud interactions. The main source of these uncertainties are dynamical processes such as turbulence and entrainment but also key aerosol parameters such as aerosol number concentration and size distribution, and to a much lesser extent, the composition. From June to August 2011 a Cloud and Aerosol Characterization Experiment (CLACE) was performed at the high-alpine research station Jungfraujoch (Switzerland, 3580 m a.s.l.) focusing on the activation of aerosol to form liquid-phase clouds (in the cloud base temperature range of -8 to $5\,°C$). With a box model the sensitivity of the effective peak supersaturation (SS_{peak}), an important parameter for cloud activation, to key aerosol and dynamical parameters was investigated. The updraft velocity, which defines the cooling rate of an air parcel, was found to have the greatest influence on SS_{peak}. Small-scale variations in the cooling rate with large amplitudes can significantly alter CCN activation. Thus, an accurate knowledge of the air parcel history is required to estimate SS_{peak}. The results show that the cloud base updraft velocities estimated from the horizontal wind measurements made at the Jungfraujoch can be divided by a factor of approximately 4 to get the updraft velocity required for the model to reproduce the observed SS_{peak}. Furthermore, there is a maximum of influence from turbulence on SS_{peak} between 0.2–0.4 %. Simulating the small-scale fluctuations with several amplitudes, frequencies and phases, revealed that independently on the amplitude, the effect of the frequency on SS_{peak} shows a maximum at 0.46 (median over all phases) and at higher frequencies, the maximum SS_{peak} decreases again. It was found that an increase in amplitude of the small-scale variations in the cooling rate, can significantly alter the CCN activation.

1 Introduction

The interactions between aerosols and clouds are the largest contributors to uncertainty in the calculation of aerosol radiative forcing (Boucher et al., 2013). Aerosols with a cer-

tain size, shape and chemical composition are able to form a cloud droplet, if they are exposed to air which is supersaturated with respect to water vapour. Particles that are able to activate and become cloud droplets are called cloud condensation nuclei (CCN). The number concentration of CCN is determined by the aerosol number size distribution, the hygroscopic properties of the aerosol and the supersaturation in the surrounding air. Thus, to address the aerosol–cloud interaction processes in detail, all these properties need to be known. However, present climate models are not capable of representing these aerosol properties in the required detail. Thus, compromises and assumptions that accurately address the most important aerosol effects within the constraints of application are required (Cherian et al., 2014; Dufresne et al., 2013; Levy et al., 2013). It has been pointed out by Boucher et al. (2013) that the main uncertainties in the aerosol radiative forcing are due to aerosol–cloud interaction dynamical factors such as turbulent strength and entrainment controlling the cloud condensation rate, and the key aerosol parameters such as aerosol number concentration and size distribution, and to a much lesser extent, the composition.

One of the properties that can be used to characterize the CCN activity of an aerosol particle is the critical supersaturation, i.e. the lowest supersaturation at which the particle is activated to a cloud droplet. The critical supersaturation depends on the particle size and chemical composition and is described by Köhler theory (Köhler, 1936). Whether a particle is able to act as a CCN in the atmosphere depends, aside from the particle's chemical and physical properties, on the supersaturation of water vapour. As an air parcel rises, it cools and may become supersaturated. Those particles with a critical supersaturation at or below the supersaturation in the air parcel will activate to form cloud droplets. The highest supersaturation that a particle experiences for a sufficiently long time to grow to a stable cloud droplet is defined as the effective peak supersaturation (SS_{peak}; Hammer et al., 2014) and this value is important as it determines the minimum activation diameter in a population of particles, and thus the number of particles which activate to form cloud droplets. Small-scale fluctuations in vertical velocity can alter the path of an air parcel and thereby also the corresponding SS_{peak}, which is dependent on the cooling rate of the air parcel.

3

The influence of physical and chemical quantities on the number and size of cloud droplets has been the subject of model studies for some time. A three dimensional model was used by Clark and Hall (1979) to examine the effect of fluctuations in super-saturation on the droplet size distribution evolution. They suggest that the observed broadening in the droplet size distribution above cloud base in cumulus clouds cannot be fully reproduced by the addition of fluctuations to a Lagrangian model, as this ignores spatial correlations between population or thermodynamic characteristics. However they also performed Lagrangian simulations for comparison with their 3D modelling results, and find that these reproduce a lower bound to the population broadening caused by turbulence. Fluctuations in saturation ratio were also investigated with a stochastic model by Kulmala et al. (1997), who pointed out that under conditions that are, on average, sub-saturated, fluctuations may lead to the activation of aerosol, and that above saturation, variation in saturation ratio may lead to accelerated growth of droplets. Feingold et al. (2003) applied an adiabatic parcel model and find that in non-precipitating stratocumulus cloud, at higher aerosol number densities (above a number corresponding to an extinction of approximately $0.008 \, \mathrm{km}^{-1}$ in their study), the updraft velocity begins to have an influence on the droplet effective radius, as more aerosol is activated and the available condensable water is shared among more growing droplets. Using a cloud parcel model, Lance et al. (2004) showed that the presence of organic surfactants enhances the sensitivity of the modelled droplet concentration to vertical wind velocity, increasing the number of droplets. Under polluted conditions, this effect was determined to be of the same scale as the influence of updraft velocity. Using data from a non-urban site, Dusek et al. (2010) have shown that the number of activated aerosol mainly depends on the details of the aerosol size distribution and not the chemical composition. An adiabatic parcel model was used by Chuang (2006) to show that aerosol activation is sensitive to the mass accommodation coefficient below values of approximately $0.1 - 0.001$, and that the sensitivity to updraft velocity is greater under polluted conditions than under conditions with low aerosol number concentrations. In the study of Partridge et al. (2012), an adiabatic cloud parcel model was used to show that under clean conditions, the number and size of aerosol in the accumulation mode was important in determining the number

4

of cloud droplets, however under polluted conditions, aerosol activation was more sensitive to chemical composition. Also, the sensitivity of the cloud droplet formation to aerosol chemical composition was found to increase when the updraft was reduced.

Ditas et al. (2012) derived the fluctuations of supersaturation in marine stratocumulus, based on observational data, finding a peak to peak supersaturation fluctuation in the range of 1.5 %. The present study builds on the work of Hammer et al. (2014), which showed that there is a strong link between SS_{peak} and the updraft velocity. Additionally, it was shown that the physical properties (number concentration and size) of the aerosol possibly also have a non-negligible influence on SS_{peak}. However, the study was not able to shed light into which extent each parameter contributed to SS_{peak}. In here a sensitivity study was performed to gain more knowledge of the contribution of different physical and chemical aerosol parameters as well as the dynamical history of the air parcel to SS_{peak}. This was done for a dedicated measurement campaign (CLACE2011; described in Sect. 2). Although only results from the campaign performed in 2011 are shown, all results shown in Sects. 3.1 and 3.2 are also applicable to the earlier campaign performed in 2010 as the chemical and physical properties of the aerosol, and the meteorological conditions encountered during the campaign were similar in 2010 and 2011 (Hammer et al., 2014).

To develop effective models, it is important to know the influence of the variation of several key aerosol parameters influencing the cloud droplet formation. It has been pointed out by Boucher et al. (2013) and Spichtinger and Cziczo (2008) that the main uncertainties in the aerosol radiative forcing are due to aerosol-cloud interaction dynamical factors such as turbulent strength and entrainment controlling the cloud condensation rate, and the key aerosol parameters such as aerosol number concentration and size distribution, and to a much lesser extent, the composition. I.e. the interplay of dynamics versus effects purely attributed to aerosols remains highly uncertain. Thus, in this study the influence of the variation of the turbulent strength and the updraft velocity on the cloud activation is investigated using a cloud parcel model.

2 Methods

2.1 Observational data

Measurements of aerosol and cloud properties were performed at the high-alpine site Jungfraujoch (3580 m a.s.l.) in Switzerland during summer 2011. This intensive measure-
5 ment campaign was carried out within the framework of a CLoud and Aerosol Characterization Experiment (CLACE) campaign. The main focus of the campaign was to investigate the physical, chemical and optical properties of aerosols as well as the interaction of the aerosol particles with clouds, for a better quantification of the radiative forcing due to aerosol–radiation interactions (RFari) and the radiative forcing due to aerosol–cloud inter-
10 actions (RFaci). These measurements provide the basis for the current modelling study.

Due to the topography around the Jungfraujoch (JFJ) mainly northwest (NW) and southeast (SE) wind directions are observed at the site. The topography approaching from the NW differs from that on the SE side as can be seen in Fig. 1. To the SE, the Great Aletsch glacier declines gradually from the JFJ (1500 m of altitude decrease over 18 km) while the
15 NW side drops steeply, descending 1500 m over a horizontal distance of 4800 m (Ketterer et al., 2014).

To make the readability of the manuscript easier, Table 1 gives an overview of all notations used in this manuscript grouped into calculated, measured and modeled parameters.

2.1.1 Measurement setup

20 A number of quantities measured at the JFJ were either used as model input directly, or were used to calculate model input parameters. These included the aerosol size distribution, the temperature and pressure, wind speed and direction, and the total water content of the air. For sampling the aerosols and the hydrometeors on JFJ, an interstitial and a total inlet were installed on the roof of the laboratory. The interstitial inlet sampled only the
25 non-activated particles by a size discriminator to remove droplets larger than 2 μm in aerodynamic diameter. In the laboratory the aerosol was dried to RH < 10 % as it was heated to

room temperature (typically 20 to 30 °C). The total inlet sampled the hydrometeors as well as the interstitial particles, i.e. all particles. The condensed water of the hydrometeors and the aerosol particles was evaporated via heating the top part of the total inlet to approximately 20 °C. Thus, all dried aerosol particles (non-activated aerosols and the residuals

5 of the cloud droplets) reached the laboratory. The difference between the number concentration measured behind the total inlet minus the number concentration measured behind the interstitial inlet corresponds to the number of cloud residuals, i.e. the number of particles that have been activated to cloud droplets. Downstream of the inlets, two scanning mobility particle sizers (SMPS) measured the total and the interstitial dry particle number

10 concentration, respectively. Additionally, a cloud condensation nuclei counter (CCNC; DMT CCNC-100, described by Roberts and Nenes, 2005) measured the polydisperse CCN number concentration at eight defined supersaturations (SS) behind the total inlet. Combining these measurements with the total dry particle number size distributions, measured with the SMPS behind the total inlet, the hygroscopicity parameter (κ) was inferred (Hammer et al.,

15 2014).

The 3-dimensional wind speed vector at the JFJ with a time resolution of 20 Hz was measured with an ultrasonic anemometer (Metek USA-1). This instrument was installed on a 3 m pole pointing away from the JFJ building to reduce the influence of the building on the measured wind fields, although this influence could not be totally eliminated. Therefore, the

20 wind direction and horizontal wind speed data of the ultrasonic anemometer were not further used in this study. Nevertheless, the high-time resolved vertical wind speed measured by the ultrasonic anemometer is still expected to provide information on the small-scale fluctuations of the air mass.

The horizontal wind direction was obtained with the rosemount pitot tube anemometer.

25 This instrument is mounted at the top of a 10 m mast located at around 75 m away from the ultrasonic anemometer. The measurements were performed as part of the SwissMetNet network of MeteoSwiss together with temperature and pressure measurements continuously obtained at the JFJ. The temperature is measured with a thermo-hygrometer Thygan VTP-37 (Meteolabor AG).

Cloud presence and LWC were measured with a particle volume monitor (PVM-100; Gerber, 1991).

2.1.2 Defined cloud periods

Cloud periods that exhibited evidence of substantial entrainment or mixing were not in-
5 cluded in the analysis. Such clouds were detected by analysing the activated fraction of the aerosol particles as a function of aerosol size. Periods where the largest size bins were not at least 90 % activated were excluded. This is the same procedure to that used by Hammer et al. (2014).

In here, only clouds reaching the JFJ with NW wind directions are considered. Relatively
10 few measurement points when when SE wind was present, and also because the clouds coming from the NW are mostly found to be formed locally by rapid updraughts, in contrast to the clouds from the south, which are often stratus, which has been advected from further away. This makes the clouds from the NW more suitable for our study.

2.1.3 Estimation of the updraft velocity at the cloud base

15 (This section is composed by a summary of section 3.4 in Hammer et al. (2014).)

It is not feasible to measure the updraft velocity at the point of aerosol activation at the JFJ. Thus, an estimate of the updraft velocity at the cloud base ($w_{\text{act}}^{\text{estim}}$) was inferred from the horizontal wind speed at the JFJ, as measured by the Rosemount pitot tube anemometer by making the following assumptions: (1) the air approaching the JFJ research station strictly
20 followed the terrain, i.e. the flow lines are parallel to the surface (at least in the lowest layers). (2) Neither horizontal convergence nor divergence of the flow lines occurred between cloud base and the JFJ. Thus, the horizontal wind speed component stays the same between cloud base and the JFJ. With these assumptions, $w_{\text{act}}^{\text{estim}}$ is obtained from the horizontal wind speed measured at the JFJ ($v_{\text{JFJ}}^{\text{h}}$):

25 $$w_{\text{act}}^{\text{estim}} = \tan(\alpha) v_{\text{JFJ}}^{\text{h}}, \tag{1}$$

8

where α denotes the inclination angle of the flow lines at cloud base. According to the topography software "Atlas der Schweiz 3.0" from Swisstopo and ETH Zurich, the terrain has a mean inclination of $\alpha \approx 46°$ over the last 700 m altitude difference before reaching the JFJ for northwesterly advection, which is close to the estimated location of the median cloud base during CLACE2011.

2.1.4 The effective peak supersaturation

The cooling of an air parcel below its dew point temperature results in the formation of a cloud. According to Köhler theory (Köhler, 1936) the equilibrium saturation vapour pressure (S_{eq}) over a solution droplet is described considering the Raoult (solute) and Kelvin laws. The critical supersaturation (SS_{crit}) of a particle with a certain size and composition (κ) defines the point of activation from particle to cloud droplet. Therefore, all particles in an air parcel having a SS_{crit} smaller than SS_{peak} are able to activate and grow to cloud droplets. In the box model the S_{eq} is calculated for each time step along the temperature and pressure on the air parcel trajectory. The maximum relative water vapour pressure between the model initialization point and the JFJ is expressed as SS_{max}^{mod}. The simulated effective peak supersaturation, SS_{peak}^{mod}, however is below SS_{max}^{mod}. SS_{peak}^{mod} was obtained by finding the highest water vapour saturation which lead to droplets larger than 2 μm in diameter. In earlier studies it was found that a diameter of 2 μm is a good threshold distinguishing the hygroscopic grown particles from cloud droplets (Jurányi et al., 2011; Henning et al., 2002).

It is important to note that in Hammer et al. (2014) the definition of the SS_{peak}^{mod} simply was the "highest SS reached along the trajectory". The new definition described above is needed for investigating the small-scale fluctuation described in Sect. 3.3.1. The comparison SS_{peak}^{mod} obtained by the two definitions respectively, was within 10 %.

The SS_{peak} was retrieved as follow: 1) the activation threshold diameter was determined from the measurements of the total and interstitial number size distributions 2) the aerosol hygroscopicity was obtained from the simultaneous CCNC measurements 3) the activation threshold diameter was combined with the aerosol hygroscopicity to infer the effective peak supersaturation. A relative uncertainty of about ±30 % was estimated for SS_{peak}. A detailed

9

description how the SS_{peak} was estimated from the measurements performed at the JFJ can be found in Hammer et al. (2014).

2.2 Box model simulations

2.2.1 Box model description (ZOMM)

The Zurich optical and microphysical model (ZOMM) was used in this study to simulate the effect of aerosol properties and atmospheric dynamics on liquid cloud formation (please note, that no ice formation was simulated). ZOMM is a box model which calculates the evolution of an initial aerosol distribution along a temperature and pressure trajectory. A further description of ZOMM can be found in Luo et al. (2003) and Hoyle et al. (2005, 2013). The model is available on request via the following e-mail: beiping.luo@env.ethz.ch.

For the initialisation of the model, the cloud periods detected at the JFJ were divided into six minute periods. Therefore, all aerosol and cloud properties described in this study are given in six minute averages. The temperature range of the observed clouds was from -8 to $5\,^{\circ}$C.

It was important to know the altitude of cloud base. The cloud base altitude was inferred from the liquid water content (LWC) of the cloud observed at the JFJ assuming an adiabatic rise of the air parcel before cloud formation. Water removal due to precipitation is negligible since it is assumed that the total water content is preserved (Hammer et al., 2014). Assuming all the water is in vapour phase, the dew point temperature, was calculated via the ideal gas law and the Clausius–Clapeyron equation (Goff and Gratch, 1946). Via the hypsometric equation, the cloud base can be determined by iteratively lowering the altitude. The cloud base was defined as the point where the water partial pressure (assuming all water is in the gas phase) is equal to the saturation vapour pressure over liquid water (corrected for the pressure difference between the cloud base and the JFJ). A detailed description can be found in Hammer et al. (2014).

The model was initialised with an aerosol size distribution, consisting of aerosol number concentrations in 100 size bins. The size distributions were taken from the SMPS mea-

surements at the total inlet, and therefore include both activated and interstitial aerosol. As ZOMM is a box model, mixing and sedimentation processes are not accounted for, and the total water content of an air parcel is conserved during the simulation. The total water contents used in the simulations were determined from the sum of the gas and liquid phase water measured at the JFJ. To initialize the model under clearly subsaturated conditions, the temperature, and the corresponding pressure on the air parcel trajectory was calculated at RH $\approx 90\%$ to the cloud base of RH $= 100\%$ assuming a dry adiabatic lapse rate of $\Gamma_{dry} = 0.98\,\text{K}\,(100\,\text{m})^{-1}$. The calculation of the temperature and the corresponding pressure on the air parcel trajectory from the cloud base to the JFJ was done assuming a wet adiabatic lapse rate of $\Gamma_{wet} = 0.65\,\text{K}\,(100\,\text{m})^{-1}$. Implicit in this initialisation is the assumption that the aerosol size distribution observed at the JFJ is the same as that which was present below the cloud base. As it is not feasible to measure the aerosol size distributions below the cloud base at the JFJ, this assumption cannot be tested. However in this study the analysis is not performed on single trajectories, rather the results of the simulations are examined together, therefore the variability of the size distributions observed at the JFJ should capture the variability of the size distributions the cloud base.

The aerosol size observed in a single SMPS measurement has an uncertainty of about 10 % Wiedersohler et al. (2012); however the input distributions used in the basic model simulations consist of median size distributions taken over the CLACE 2011 campaign. The bin resolution used in the model is the same as that measured by the SMPS. Any uncertainties in the model calculation resulting from the resolution of the bin sizes or the aerosol size distribution would be much smaller than the differences in simulated peak supersaturation caused by varying the number and size of the aerosols, as is done in Fig. 6.

Below saturation with respect to liquid water, the hygroscopic growth, i.e. water content of the aerosol is calculated according to the κ–Köhler parametrization of (Petters and Kreidenweis, 2007), i.e. equation, under the assumption of equilibrium between the gas and liquid phases:

$$S(D,\kappa) = \frac{D^3 - D_{dry}^3}{D^3 - D_{dry}^3(1-\kappa)} \exp\left(\frac{4\sigma_{s/a}M_w}{RT\rho_w D}\right), \tag{2}$$

11

where D is the droplet diameter, D_{dry} the dry diameter, $\sigma_{s/a}$ the surface tension of the solution/air interface, M_w the molar mass of water, R the ideal gas constant, T the prevailing air temperature and ρ_w the density of water.

At $S > 0.99$ with respect to liquid water, or at high cooling rates, the kinetic uptake of water to the droplets from the gas phase is calculated, accounting for gas phase diffusion as well as the Kelvin effect. The new radius of each size bin is calculated, and the bins are allowed to evolve independently in radius space, i.e. they are not constrained to a particular distribution shape.

The simulation follows the time series of temperature and pressure values which is given as input, and the simulation ends once the conditions observed at the JFJ are reached. In this way, the number of activated droplets and the effective peak supersaturation predicted by the model can be compared with the values determined from the JFJ observational data. The threshold is, therefore, defined on final droplet size but on the threshold of the droplet size at the point droplets grow fast (i.e. at point of activation).

2.3 Investigated parameters

2.3.1 Simulated small-scale temperature fluctuations

To investigate the influence of the small-scale fluctuations of SS_{peak} on the temperature (T_{turb}) and pressure along the air parcel trajectory from the initialization point to the JFJ at time (t), the 20 Hz time resolved updraft velocities measured by the sonic anemometer (w_{act}^{meas}) were applied to the linear temperature decrease derived from the lapse rate (T_{lin}). This was done by superimposing a time series of temperature fluctuations measured at the JFJ upon the linear temperature trajectory along which the model was run (see black line in Fig. 2). The time series of fluctuations was chosen to be simply that which was measured at the JFJ during the time taken for the air parcel to ascend from the point where the model was initialized (indicated in Fig. 2 with RH=90%), to the JFJ (indicated in Fig. 2 with JFJ). The relative vertical fluctuation calculated from the measured wind field at the JFJ (w') at

12

time t was retrieved as follows:

$$w'(t) = w_{\text{act}}^{\text{meas}}(t) - (a + bt), \tag{3}$$

where a and b are the y intercept and the slope, respectively, from the linear regression function of $w_{\text{act}}^{\text{meas}}(t)$ for the time period from t_{start} (the time at which the model was ini-

5 tialized) to t_{JFJ} (the time at which the modelled trajectory reached the JFJ). The deviation from $T_{\text{lin}}(t)$ due to the fluctuation ($T_{\text{turb}}'(t)$) was then calculated by multiplying $w'(t)$ with the wet adiabatic lapse rate ($\Gamma_{\text{wet}} = 0.65\,\text{K}\,(100\,\text{m})^{-1}$. Adding $T_{\text{turb}}'(t)$ to $T_{\text{lin}}(t)$ leads then to $T_{\text{turb}}(t)$. $T_{\text{turb}}'(t)$ ranged from -0.8 to $1.1\,\text{K}$ with a 25th percentile of $0.01\,\text{K}$, a 75th percentile of $0.05\,\text{K}$ and a median of $0.03\,\text{K}$. Figure 2 shows an example of T_{turb} for the model

10 run detected at the JFJ on 8 August 2011 18:20 UTC.

2.3.2 Modelled updraft velocity

As well as being estimated from measurements (see Sect. 2.1.3), the updraft velocity can be modelled ($w_{\text{act}}^{\text{mod}}$). With the ZOMM model, an initial model run was performed, and the number of simulated cloud droplets was compared with the observed number of cloud residuals

15 at the JFJ. The cooling rate in the model was then iteratively adjusted until the simulated number of droplets was within 2 % of the observed number of cloud residuals, which was considered to be sufficient for the propagation of SS_{peak} values.

The modelled updraft velocity, $w_{\text{act}}^{\text{mod}}$, was used for the reference model simulation (see Sect. 2.4). This parameter, $w_{\text{act}}^{\text{mod}}$, was then varied to investigate the sensitivity of the updraft

20 velocity on SS_{peak} (see results in Sect. 3.2).

2.3.3 Aerosol- and updraft-limited regimes

Previous studies have found that a high SS_{peak} can be caused by a high updraft velocity or a low number of potential CCN (i.e. low number concentration of sufficiently large particles and/or low particle hygroscopicity). Conversely, a low SS_{peak} can be caused by small updraft

25 velocity or a large number of potential CCN (i.e. high number concentration of large particles and/or high particle hygroscopicity). The study of Reutter et al. (2009) defined three

13

different regimes depending on the ratio between the updraft velocity and the particle number concentration (w/N_{CN}): (1) the aerosol-limited regime, (2) the updraft-limited regime and (3) the aerosol- and updraft-sensitive regime (transitional regime). The aerosol-limited regime is characterized by a relatively high ratio of w/N_{CN}, by a high activated fraction of
5 aerosol particles (larger than 90 %) and the aerosol-limited regime is basically independent of w. The high updraft velocities lead to high SS_{peak} large enough to activate almost all of the particles except of the very small ones. The updraft-limited regime is characterized by a low ratio of w/N_{CN} (smaller than 20 %), saying that only a few particles are activated to cloud droplets due to low SS_{peak} values. In this regime the cloud droplet number con-
10 centration exhibits a linear dependence on w and a weak dependence on the N_{CN}. The aerosol- and updraft-sensitive regime is characterized by w/N_{CN} values lying between the two other regimes. Depending on SS_{peak}, the critical dry activation diameter for CCN activation ranges from very low up to the maximum of the dry particle size distribution. All these regimes will be discussed in Sect. 3.2 regarding the sensitivity study of SS_{peak} on
15 updraft velocity, particle size distribution and hygroscopicity. Thereby, the aerosol number concentration and size was varied by ± 15 % to investigate the sensitivity of the aerosol- and updraft-limited regimes on SS_{peak} (see results in Sect. 3.2).

2.3.4 Hygroscopicity parameter

The hygroscopicity parameter, κ, stays rather constant over time at the Jungfraujoch at
20 around 0.2 (Jurányi et al., 2011). To investigate the sensitivity of κ on SS_{peak}, a typical κ value for an aerosol size distribution with a larger fraction of organics ($\kappa = 0.1$; Dusek et al., 2010) and for a continental aerosol ($\kappa = 0.3$; Andreae and Rosenfeld, 2008; Pringle et al., 2010) was used (see results in Sect. 3.2). It is important to note, that the studies Hammer et al. (2014) and Hammer et al. (2014) revealed only a small influence of the κ value on the
25 calculated SS_{peak}.

14

2.4 Reference model for sensitivity analysis

For the sensitivity studies shown in Sects. 3.2 and 3.3.1 a set of reference model simulations was used. These reference simulations were performed using the dataset measured at the JFJ during CLACE2011 as input variables. For this purpose an average, constant κ value

[5] of 0.2 was used (Jurányi et al., 2011). For the updraft velocity, the simulated parameter w_{act}^{mod} was used as described in Sect. 2.3.2. All output parameters of the reference model simulations are depicted with a superscript ^{ref}, as e.g. for the effective peak supersaturation from the reference model simulation: SS_{peak}^{ref}.

3 Results and discussions

[10] The sensitivity of the SS_{peak} to the particle's size distribution and hygroscopicity, cooling rate of the air parcel (i.e. updraft velocity), and the temperature fluctuations with time have been investigated.

3.1 Comparison of the estimated and the simulated updraft velocity

The study of Hammer et al. (2014) simulated SS_{peak} using w_{act}^{estim} as an upper limit for the
[15] updraft velocity at the point of aerosol activation (see Sect. 2.1.3) and the same model as in this study. It was observed that SS_{peak} was generally overestimated for a particular w_{act}^{estim} (see Fig. 3; red circles and black line). It was speculated that the estimated w_{act}^{estim} might overestimate the true updraft velocity at cloud base due to flow convergence in the approach to the narrow gap in which the JFJ is located (see Fig. 1), or due to flow lines
[20] that do not strictly follow the terrain. Thus, in the present work, the mean updraft velocity was simulated with ZOMM, as described in Sect. 2.3.2. In Fig. 4 the ratio of the modelled mean updraft velocity (w_{act}^{mod}) to w_{act}^{estim} is shown for each model simulation. The ratios show that w_{act}^{mod} is a factor of 4 (median) lower than the estimated w_{act}^{estim}. In Fig. 3, the red dots show data from Hammer et al. (2014), where the effective peak supersaturation was plotted
[25] against the estimated updraft velocity, w_{act}^{estim}. There, it was found that there was a very

15

weak correlation between updraft velocity and SS_{peak}^{estim} (derived from measurements; see Sect. 2.1.4). The modelled data points are substantially closer to the model simulations when w_{act}^{mod} (green circles) rather than w_{act}^{estim} (red circles), is plotted against SS_{peak}^{estim} as w_{act}^{mod} was calculated by constraining the model to the observed number of activated droplets, which is related to SS_{peak}. The fact that when the model is constrained to reproduce the observed number of droplets, a lower updraft velocity is found, causing a better agreement between modelled and estimated SS_{peak}, suggests that the updraft velocity estimated from wind speed measurements at the JFJ is indeed overestimated.

The black curves in Fig. 3 represent the box model simulations of SS_{peak}^{mod} obtained by running the simulations for a range of constant updraft velocities. In the upper line, the aerosol size distribution was chosen so that the number and sizes of the aerosol and κ value were representative of the 75th percentile of those observed during CLACE 2011. The bottom line was calculated similarly using aerosol properties representative of the 25th percentile, with the middle line calculated using aerosol properties representative of the median. From this, the expected effect of SS_{peak} on updraft velocity can be seen. The black line lies near the middle of the cloud of green points, and the variability of the green circles about the line is a result of the different chemical and physical properties of the aerosol distributions in the different model simulations. The dashed curves represent the box model simulations of SS_{peak}^{mod} using the 25th and the 75th percentiles of the aerosol properties from CLACE2011 (see values in Table 2). While the data points showing the SS_{peak}^{estim} values derived from measurements vs. the w_{act}^{estim} values are spread across the upper left half of the plot, the relationship between SS_{peak}^{mod} and w_{act}^{mod} appears better defined, and the points shift substantially closer towards the black line, with 39 % being between the 25th and 75th percentile band of the values modelled with fixed aerosol size distributions. This substantial shift in the data illustrates the strong influence that the vertical wind most likely has on the SS_{peak}.

16

3.2 Influence of the updraft velocity, particle size distribution and hygroscopicity on the effective peak supersaturation

According to previous studies, a low SS_{peak} can be caused by small updraft velocity or a large number of potential CCN. Conversely, a high SS_{peak} can be caused by a high updraft velocity or a low number of potential CCN (see Sect. 2.3.3).

In Sect. 3.1 it was shown that w_{act}^{mod} is on average a factor of 4 lower than the estimated w_{act}^{estim}. This difference can most likely be explained by the fact that w_{act}^{estim} is an upper limit for the updraft velocity and w_{act}^{mod} is based on the simulated number of cloud droplets and the number of cloud residuals at the JFJ (as described in Sect. 2.3.2). Thus, w_{act}^{mod} is not an upper limit but the "true" updraft velocity at the point of aerosol activation. To investigate the sensitivity of SS_{peak} to the updraft velocity, the modelled value w_{act}^{mod} was divided by 2 (w_{mod}^{div2}), divided by 5 (w_{mod}^{div5}), multiplied by 2 (w_{mod}^{mul2}) and 5 (w_{mod}^{mul5}). The ratio 5 describes the maximum deviation from the mean value of w_{act}^{mod} and the ratio 2 is given from the 75th and 25th percentile of w_{act}^{mod}, which are about a factor of 2 from the mean value. Figure 5 shows the ratio of $SS_{peak}(w_{mod}^{mulx})$ using the modified updraft velocities as input parameters to the SS_{peak}^{ref} using the input parameter w_{act}^{mod}. All symbols are colour coded to show the number concentration in the size range of 96 (median dry activation diameter for CLACE2011) and 500 nm (upper limit of the SMPS). This value was used as an estimate for the potential CCN number concentration. It was found that using w_{mod}^{div2} as input parameter, SS_{peak}^{ref} is lowered on average by 25 % and using w_{act}^{div5} as input parameter lowers SS_{peak}^{ref} on average by 50 %. Using w_{mod}^{mul2} as input parameter the SS_{peak}^{ref} is raised by 38 % and with w_{mod}^{mul5} the SS_{peak} is on average a factor of 2 larger compared to using w^{ref} (i.e. w_{act}^{mod}) as input parameter. Therefore, the relative influence of small and large changes in the updraft velocity is similar. Furthermore, an increase of the influence of w_{act}^{mod} from low to high SS_{peak}^{ref} on SS_{peak} was observed. Low SS_{peak} values are less affected by the updraft velocity because for low SS_{peak} values w_{act}^{mod} is already relatively low and therefore the absolute difference in w_{act}^{mod} due to a division by 2 or 5 is rather small and the rate of increase in saturation will not change substantially. Comparable to the aerosol-limited regime (Reutter et al., 2009) Fig. 5

17

shows that the effect of changes in w_{act} is slightly larger when the potential CCN number concentration is lower. Thus, the ratio of w/N_{CN} at these low SS_{peak} values is relatively low (at about 0.003) and is increasing with an increase in $SS_{\text{peak}}^{\text{ref}}$ (up to about 0.03). This corresponds well with the results presented by Chuang (2006), and Feingold et al. (2003), who

[5] both found that under more polluted conditions, the characteristics of the droplet distribution are more sensitive to changes in the updraft velocity. In addition, the sensitivity of the peak supersaturation to a doubling (or increase by a factor of 5) in vertical wind velocity is slightly greater than the sensitivity to the corresponding decrease. This is similar to the findings of Partridge et al. (2012) for cloud droplet number concentration.

[10] In Sect. 2 it is described that the topography at the JFJ defines two main wind directions, NW and SE wind. The variability of the particle number concentration as well as the particle size is expected to be on the same order of magnitude as the difference between NW and SE wind case. The dry number size distributions for the SE wind case during CLACE2011 showed on average 15 % higher particle number concentration and 15 % larger particles

[15] than when the wind came from the NW. Thus, for the sensitivity of $SS_{\text{peak}}^{\text{ref}}$ to the dry particle number size distribution the measured particle number size distribution was used as an input for the model simulations applying a 15 % higher and lower particle number concentration and a 15 % increase and decrease in diameter across all size bins, respectively (see Fig. 6). The effects of changing the particle number size distribution and the particle

[20] number concentration were investigated separately. The higher/lower number concentration of larger particles decreases/raises the $SS_{\text{peak}}^{\text{ref}}$, respectively. The same was found for larger/smaller particle number concentration. 15 % smaller and higher particle number concentration change the modelled peak supersaturation by approximately ± 8 %, compared to the reference case. This ratio is rather constant over the whole diameter range. Using

[25] a 15 % smaller and larger size distribution compared to the reference, a maximum difference of 21 % was observed, however above a $SS_{\text{peak}}^{\text{ref}}$ of about 0.4, the effect of changing the size or the number of the particles is similar.

It is interesting to note that while changing the number of the particles has a relatively constant effect on the modelled SS_{peak}, changing the size of the particles has a much more

18

pronounced effect at low SS_{peak}^{ref}. This is because changing the size of the particles changes the minimum supersaturation at which the particles can activate. At low SS_{peak}^{ref}, updrafts are generally smaller (colour coding in Fig. 6), and only the largest particles activate. If they are smaller (larger) SS_{peak} will be higher (lower). At higher SS_{peak}^{ref}, where the updrafts

5 are generally higher, the critical saturation of the largest particles plays less of a role in determining the SS_{peak}. Changing the number of the particles on the other hand does not affect the critical saturation needed to activate the largest particles, but rather influences just the condensation sink once the critical saturation has been exceeded (Rogers and Yau, 1989). Therefore the effect is relatively constant across the range of SS_{peak}^{ref}.

10 Another aerosol parameter influencing SS_{peak} is the hygroscopicity parameter of the dry particles, κ, describing the Raoult term of the Köhler equation (Petters and Kreidenweis, 2007). At the Jungfraujoch, it stays rather constant over time (Jurányi et al., 2011; Hammer et al., 2014) at $\kappa \approx 0.2$. To look into the sensitivity of SS_{peak} to κ, a typical κ value for an aerosol size distribution with a larger fraction of organics ($\kappa = 0.1$; Dusek et al., 2010) and

15 for a continental aerosol ($\kappa = 0.3$; Andreae and Rosenfeld, 2008; Pringle et al., 2010) was used as input for the model simulation. For the reference model simulation a $\kappa = 0.2$ was used as input. Applying the aerosol size distribution with $\kappa = 0.3$ as input for the model simulation results in lower SS_{peak} values compared to the reference size distribution (SS_{peak}^{ref}; see Fig. 7). On average the SS_{peak} is lowered by 6 %, however, for smaller SS_{peak}^{ref} the effect

20 of a larger κ value is stronger and lowers the SS_{peak} up to 15 %. The model simulations using a κ value of 0.1 show on average 11 % higher SS_{peak} values compared to the reference model simulation, whereas the maximum difference lies at 30 %. The larger increase of ratios of $SS_{peak}(\kappa = 0.1) : SS_{peak}^{ref}$ compared to the decrease for $SS_{peak}(\kappa = 0.3) : SS_{peak}^{ref}$ can be explained by the fact that a lower particle hygroscopicity results in a lower conden-

25 sation of water vapour onto the particles and thus particles reach the size where the Kelvin term of the Köhler theory (Petters and Kreidenweis, 2007) becomes more important than the Raoult term and where particles activate to cloud droplets at larger sizes compared to higher particle hygroscopicity. The stronger influence of κ on small SS_{peak} values can be explained by the same reason as for the smaller/larger particle number concentration: at

the small updraft velocities associated with small SS_{peak} (see Fig. 7), the critical saturation at which the largest particles activate plays a more important role in determining the final SS_{peak} than it does at higher updraft velocities. The changes in κ result in changes in this critical saturation, therefore the changes in κ have a larger effect at low SS_{peak}^{ref}.

3.3 Turbulence estimations and its influence on the effective peak supersaturation

3.3.1 Measured turbulence

Turbulence is often present before cloud formation and within clouds. To address the influence of turbulence on the cloud activation, i.e. on the effective peak supersaturation, the linear cooling rate was modulated with the fluctuations obtained by a ultrasonic anemometer (Metek USA-1) that was located close to the other instruments at the site as described in Sect. 2.3.1. Figure 8 shows the ratio of $SS_{peak}^{fluc \cdot x}$ modelled applying the real-time fluctuations with a factor (x) to the cooling rate vs. SS_{peak}^{ref} using a linear cooling rate (reference model simulation). It was assumed that each particle experienced the same real-time fluctuations. Figure 8 shows that with stronger small-scale fluctuations (i.e. a larger x added to the fluctuation) the SS_{peak} increases significantly: applying the real-time fluctuation to the cooling rate raises the SS_{peak} by $\sim 8\%$ (shown in Fig. 8 with the ratio of $SS_{peak}^{fluc} : SS_{peak}^{ref}$). Multiplying the small-scale fluctuation added to the cooling rate by a factor of 5 increases the SS_{peak} by $\sim 87\%$ and multiplying the fluctuations by 10 increases the SS_{peak} by a factor of ~ 3.22 (see green and blue triangles in Fig. 8, respectively). The factors 5 and 10 are resulting in a similar range of temperature amplitudes used for the sinus curve simulations described in Sect. 3.3.2.

A dependence of the ratios on SS_{peak}^{ref} was observed. There is a maximum of the ratios at SS_{peak}^{ref} between 0.2–0.4 %. The smaller ratios at higher $SS_{peak}^{ref} \gtrsim 0.2\%$ are likely because fluctuations added to high cooling rates have a smaller relative influence on the cooling rate at the point of aerosol activation (updraft-limited regime; Reutter et al., 2009) than small-scale temperature fluctuations added to a small linear cooling rate. The reason for the smaller influence of the fluctuations in the air parcel for low $SS_{peak}^{ref} \lesssim 0.2\%$ is likely due

to the competition between the influence of cooling rates and aerosol properties (aerosol-limited regime; Reutter et al., 2009). Aerosol properties such as hygroscopicity, number and size are more important at lower cooling rates and thus lead to this maximum of the ratios $SS_{peak}^{fluc, x} : SS_{peak}^{ref}$ for $0.2\% \lesssim SS_{peak}^{ref} \lesssim 0.4\%$. Nevertheless, there is also a spread of the ratio at a given SS_{peak}^{ref}. This is explained by the variable nature of the temperature fluctuations – at the point where aerosol activation occurs, the cooling rate will sometimes be greatly modified by the temperature fluctuation, in some cases it will be rather close to the average cooling rate. In the latter case, the SS_{peak} from the simulation including fluctuations will be close to the SS_{peak} calculated from the reference simulation

Figure 3 showed that for small w_{act}^{mod} the model was slightly underestimating the SS_{peak}. However, including small-scale fluctuations slightly improves the SS_{peak}^{fluc}–w_{act}^{mod}-relationship at lower updraft velocities as can be seen in Fig. 9. At updrafts of 0.1 to $5\,s^{-1}$, the SS_{peak}^{fluc} to w_{act}^{mod} relationship is improved slightly, with 44% of the points lying within the range of the 25-75th percentile of the measured values, compared with 40% when fluctuations are not included.

3.3.2 Sinus curve simulations of the effective peak supersaturation

Figure 10 shows the dependency of SS_{peak} on simulated small-scale fluctuations added to the cooling rate using a certain frequency (f), amplitude (A) and phase (ϕ). Three different amplitudes ($A = 0.015$, 0.022 and 0.04 K) were used to simulate the small-scale fluctuations. The applied frequencies are in the range of 0.05 to 20 Hz. The variability on the y axis per f is given by the different phases of the sinus functions. They are in the range of 0 to $360°$ with $18°$ steps. Independently of the amplitude, the influence of the frequency on $SS_{peak}^{fluc,sin}$ shows a maximum at $f = 0.46$ Hz. Thus, the influence of $f < 0.46$ on SS_{peak} is decreasing since f is too small to affect the cooling rate. For $f > 0.46$, the influence of f on $SS_{peak}^{fluc,sin}$ is decreasing since the fluctuation is faster than the time required for significant droplet growth. Likely for the same reason the range of $SS_{peak}^{fluc,sin}$ (25th and 75th percentiles) implied by the different phases is decreasing after the maximum of $f = 0.46$ Hz. It was also

found that larger amplitudes imply a larger range of f affecting the $SS_{peak}^{fluc,sin}$ as seen in Fig. 10. Furthermore, an increase in amplitude reveals an exponential increase in $SS_{peak}^{fluc,sin}$ value (see Fig. 11).

Several combinations of amplitudes and frequencies for sinus functions were found being

5 able to represent the median small-scale fluctuations in the vicinity of the JFJ. Figure 12 shows the relationship of the modelled SS_{peak} applying simulated small-scale fluctuations to the cooling rate ($SS_{peak}^{fluc,sin}$) and SS_{peak}^{fluc}. The simulation of the small-scale fluctuations for the cooling rate was done using the example: $A = 0.24\,K$, frequency $f = 0.022\,s^{-1}$. The good linear correlation (slope $= 0.85$, intercept $= 0.06$, $r^2 = 0.88$) indicates that the combination

10 of this amplitude and frequency is able to simulate the median small-scale fluctuations in the vicinity of the JFJ.

4 Conclusions

A sensitivity analysis was performed for the cloud activation at the high-alpine research station Jungfraujoch in Switzerland. The Zurich optical microphysical model (ZOMM) was

15 used to simulate the effective peak supersaturation within the clouds using a set of input parameters, representative of the ambient air and aerosol properties at the JFJ during CLACE2011.

The analysis shows that SS_{peak} depends mainly on the updraft velocity, and not the physical properties of the aerosol. However, it is also the most difficult parameter to measure.

20 It was observed that reducing the modelled updraft velocity, w_{act}^{mod}, by a factor of 2 lowers the SS_{peak} values on average by 25 %, whereas a factor of 5 lowers the SS_{peak} on average by 50 %. While multiplying w_{act}^{mod} by a factor of 2 and 5, increases the SS_{peak} by a factor of ~ 1.38 and ~ 2, respectively. Thus, lowering or raising the updraft velocity to the same extent results in a similar influence on SS_{peak}.

25 Another input parameter influencing the SS_{peak}, is the shape of the aerosol size distribution and its hygroscopicity. The sensitivity analysis showed that representative aerosol size

22

distributions for the JFJ are influencing SS_{peak} only to a small extent up to 21 %. It was observed that the 15 %-change in particle size had a stronger influence on the SS_{peak} values at lower updraft velocities than the 15 %-change in number concentration. The influence of the hygroscopicity on SS_{peak} was investigated by taking $\kappa = 0.1$, as a typical value for a high

5　organic fraction, and by taking $\kappa = 0.3$ as a typical value for continental aerosols, as input parameter compared to the typical observed κ at the JFJ of 0.2. The average difference to the reference simulation was only $\sim \pm 10$ %, whereas the maximum difference goes up to $\sim \pm 30$ %. The lower κ showed a stronger influence on SS_{peak} compared to the higher one.

　　Small-scale temperature variations are always present at cloud formation processes. In

10　this study the influence of small-scale variations on SS_{peak} was investigated by applying real-time fluctuations, measured with an ultrasonic anemometer, to the cooling rate. Although the fluctuations were measured at the JFJ, it is assumed that conditions that lead to greater fluctuations at the JFJ also lead to greater fluctuations at cloud base. Generally, it was found that small values of SS_{peak}^{ref} between approximately 0.2 and 0.4 % are more

15　strongly influenced by small–scale variations. The decreasing influence of the small-scale fluctuations on $SS_{peak}^{ref} \gtrsim 0.4$ % could be explained due to the larger cooling rates which are less affected by small-scale variations. The decrease of the influence of the small-scale fluctuations on $SS_{peak}^{ref} \lesssim 0.2$ % is likely due to the higher competition of the small cooling rates with the aerosol properties, i.e. at these low SS_{peak}^{ref} values the aerosol properties

20　such as hygroscopicity, number concentration and size become more important. On average small-scale variations of temperature raise the SS_{peak} values to a larger extent than the other investigated parameters in this study: Multiplying the real-time fluctuation by a factor of 5 increases the SS_{peak} by ~ 87 % and multiplying the fluctuations by 10 increases the SS_{peak} by a factor of ~ 3.22 compared to conditions without any small-scale fluctuations.

25　　Simulating the small-scale fluctuations with several amplitudes, frequencies and phases, revealed that independently on the amplitude, the effect of the frequency on SS_{peak} shows a maximum at 0.46 (median over all phases). It was found that an increase in amplitude of the small-scale variations in the cooling rate, can significantly alter the CCN activation. Furthermore, small-scale fluctuations in the vicinity of the Jungfraujoch were simulated based

on several sinus functions with combinations of amplitudes and frequencies. The amplitudes are in the range of 0.01 and 0.09 K and the frequencies in the range of 0.05 and $0.24\,s^{-1}$.

Summarizing, small-scale temperature fluctuations are revealed to be the strongest effect on cloud formation processes beside the updraft velocity, which is influenced by the temperature fluctuations. The variation of aerosol number concentration and hygroscopic properties occurred to be less influenced compared to the aerosol size. Thus, this study revealed that of all investigated parameters the small-scale temperature fluctuation accompanied with the updraft velocity and the variation of aerosol size distribution has the strongest influence of cloud formation process (i.e. effective peak supersaturation).

References

Andreae, M. O. and Rosenfeld, D.: Aerosol–cloud–precipitation interactions. Part 1. The nature and sources of cloud-active aerosols, Earth-Sci. Rev., 89, 13–41, doi:10.1016/j.earscirev.2008.03.001, 2008.

Boucher, O., Randall, D., Artaxo, P., Bretherton, C., Feingold, G., Forster, P., Kerminen, V.-M., Kondo, Y., Liao, H., Lohmann, U., Rasch, P., Satheesh, S. K., Sherwood, S., Stevens, B., and Zhang, X.: Cloud and aerosols, in: Climate Change 2013: The Physical Science Basis. Contribution of Working Group I to the Fifth Assessment Report of the Intergovernmental Panel on Climate Change, Cambridge University Press, Cambridge, UK and New York, NY, USA, 2013.

24

Cherian, R., Quaas, J., Salzmann, M., and Wild, M.: Pollution trends over Europe constrain global aerosol forcing as simulated by climate models, Geophys. Res. Lett., 41, 2176–2181, doi:10.1002/2013GL058715, 2014.

Chuang, P.Y.: Sensitivity of cloud condensation nuclei activation processes to kinetic parameters, Geophys. Res. Atmos., 111, doi:10.1029/2005JD006529, 2006.

Ditas, F., Shaw, R. A., Siebert, H., Simmel, M., Wehner, B., and Wiedensohler, A.: Aerosols-cloud microphysics- thermodynamics-turbulence: evaluating supersaturation in a marine stratocumulus cloud, Atmos. Chem. Phys., 12, 2459-2468, doi:10.5194/acp-12-2459-2012, 2012.

Dufresne, J.-L., Foujols, M.-A., Denvil, S., Caubel, A., Marti, O., Aumont, O., Balkanski, Y., Bekki, S., Bellenger, H., Benshila, R., Bony, S., Bopp, L., Braconnot, P., Brockmann, P., Cadule, P., Cheruy, F., Codron, F., Cozic, A., Cugnet, D., Noblet, N., Duvel, J.-P., Ethé, C., Fairhead, L., Fichefet, T., Flavoni, S., Friedlingstein, P., Grandpeix, J.-Y., Guez, L., Guilyardi, E., Hauglustaine, D., Hourdin, F., Idelkadi, A., Ghattas, J., Joussaume, S., Kageyama, M., Krinner, G., Labetoulle, S., Lahellec, A., Lefebvre, M.-P., Lefevre, F., Levy, C., Li, Z., Lloyd, J., Lott, F., Madec, G., Mancip, M., Marchand, M., Masson, S., Meurdesoif, Y., Mignot, J., Musat, I., Parouty, S., Polcher, J., Rio, C., Schulz, M., Swingedouw, D., Szopa, S., Talandier, C., Terray, P., Viovy, N., and Vuichard, N.: Climate change projections using the IPSL-CM5 Earth System Model: from CMIP3 to CMIP5, Climate Dyn., 40, 2123–2165, doi:10.1007/s00382-012-1636-1, 2013.

Dusek, U., Frank, G. P., Curtius, J., Drewnick, F., Schneider, J., Kürten, A., Rose, D., Andreae, M. O., Borrmann, S., and Pöschl, U.: Enhanced organic mass fraction and decreased hygroscopicity of cloud condensation nuclei (CCN) during new particle formation events, Geophys. Res. Lett., 37, 1944–8007, doi:10.1029/2009GL040930, 2010.

Feingold, G., Eberhard, W.L., Veron, D.E., Previdi, M.: First measurements of the Twomey indirect effect using ground-based remote sensors, Geophys. Res. Lett., 30, 6, doi:0.1029/2002GL016633, 2003.

Gerber, H.: Supersaturation and droplet spectral evolution in fog, J. Atmos. Sci., 48, 2569–2588, doi:10.1175/1520-0469(1991)048<2569:SADSEI>2.0.CO;2, 1991.

Goff, J. A. and Gratch, S.: Low-pressure properties of water from -160 to $212\,F$, Trans. Amer. Soc. Heat. Vent. Eng., 51, 125–164, 1946.

Hammer, E., Bukowiecki, N., Gysel, M., Jurányi, Z., Hoyle, C. R., Vogt, R., Baltensperger, U., and Weingartner, E.: Investigation of the effective peak supersaturation for liquid-phase clouds at the high-alpine site Jungfraujoch, Switzerland (3580 m a.s.l.), Atmos. Chem. Phys., 14, 1123–1139, doi:10.5194/acp-14-1123-2014, 2014.

Hammer, E., Gysel, M., Roberts, G. C., Elias, T., Hofer, J., Hoyle, C. R., Bukowiecki, N., Dupont, J.-C., Burnet, F., Baltensperger, U., and Weingartner, E.: Size-dependent particle activation properties in fog during the ParisFog 2012/13 field campaign, Atmos. Chem. Phys., 14, 10517–10533, doi:10.5194/acp-14-10517-2014, 2014.

Clark, T., Hall, WD.: A numerical experiment on stochastic condensation theory, J. of Atmos. Sci., 36, 3, 470–483, 1979.

Henning, S., Weingartner, E., Schmidt, S., Wendisch, M., Gaggeler, H. W., and Baltensperger, U.: Size-dependent aerosol activation at the high-alpine site Jungfraujoch (3580 m a.s.l.), Tellus B, 54, 82–95, doi:10.1034/j.1600-0889.2002.00299.x, 2002.

Hoyle, C. R., Luo, B. P., and Peter, T.: The origin of high ice crystal number densities in cirrus clouds, J. Atmos. Sci., 62, 2568–2579, doi:10.1175/JAS3487.1, 2005.

Hoyle, C. R., Engel, I., Luo, B. P., Pitts, M. C., Poole, L. R., Grooß, J.-U., and Peter, T.: Heterogeneous formation of polar stratospheric clouds – Part 1: Nucleation of nitric acid trihydrate (NAT), Atmos. Chem. Phys., 13, 9577–9595, doi:10.5194/acp-13-9577-2013, 2013.

Juránii, Z., Gysel, M., Weingartner, E., Bukowiecki, N., Kammermann, L., and Baltensperger, U.: A 17 month climatology of the cloud condensation nuclei number concentration at the high alpine site Jungfraujoch, J. Geophys. Res.-Atmos., 116, 2156–2202, doi:10.1029/2010JD015199, 2011.

Ketterer, C., Zieger, P., Bukowiecki, N., Collaud Coen, M., Maier, O., Ruffieux, D., and Weingartner, E.: Investigation of the planetary boundary layer in the Swiss Alps using remote sensing and in situ measurements, Bound.-Lay. Meteorol., 151, 317–334, doi:10.1007/s10546-013-9897-8, 2014.

Köhler, H.: The nucleus in and the growth of hygroscopic droplets, T. Faraday Soc., 32, 1152–1161, doi:10.1039/TF9363201152, 1936.

Kulmala, M., Laaksonen, A., Charlson, R.J. and Korhonen, P.: Clouds without supersaturation, Nature, 388, 336–337, 1997.

Lance, S., Nenes, A., and Rissman, T.A.: Chemical and dynamical effects on cloud droplet number: Implications for estimates of the aerosol indirect effect, J. Geophys. Res., 109, doi:10.1029/2004JD004596,2004.

Levy, H., Horowitz, L. W., Schwarzkopf, M. D., Ming, Y., Golaz, J.-C., Naik, V., and Ramaswamy, V.: The roles of aerosol direct and indirect effects in past and future climate change, J. Geophys. Res.-Atmos., 118, 4521–4532, doi:10.1002/jgrd.50192, 2013.

26

Luo, B. P., Voigt, C., Fueglistaler, S., and Peter, T.: Extreme NAT supersaturations in mountain wave ice PSCs: A clue to NAT formation, J. Geophys. Res., 108, 4441, doi:10.1029/2002JD003104, D15, 2003.

Partridge, D. G., Vrugt, J. A., Tunved, P., Ekman, A. M. L., Struthers, H., and Sorooshian, A.: Inverse modelling of cloud-aerosol interactions – Part 2: Sensitivity tests on liquid phase clouds using a Markov chain Monte Carlo based simulation approach, Atmos. Chem. Phys., 12, 2823-2847, doi:10.5194/acp-12-2823-2012, 2012.

Petters, M. D. and Kreidenweis, S. M.: A single parameter representation of hygroscopic growth and cloud condensation nucleus activity, Atmos. Chem. Phys., 7, 1961–1971, doi:10.5194/acp-7-1961-2007, 2007.

Pringle, K. J., Tost, H., Pozzer, A., Pöschl, U., and Lelieveld, J.: Global distribution of the effective aerosol hygroscopicity parameter for CCN activation, Atmos. Chem. Phys., 10, 5241–5255, doi:10.5194/acp-10-5241-2010, 2010.

Reutter, P., Su, H., Trentmann, J., Simmel, M., Rose, D., Gunthe, S. S., Wernli, H., Andreae, M. O., and Pöschl, U.: Aerosol- and updraft-limited regimes of cloud droplet formation: influence of particle number, size and hygroscopicity on the activation of cloud condensation nuclei (CCN), Atmos. Chem. Phys., 9, 7067–7080, doi:10.5194/acp-9-7067-2009, 2009.

Roberts, G. C. and Nenes, A.: A continuous-flow streamwise thermal-gradient CCN chamber for atmospheric measurements, Aerosol Sci. Tech., 39, 206–221, doi:10.1080/027868290913988, 2005.

Rogers, R. and Yau, M.: A Short Course in Cloud Physics, International Series in Natural Philosophy, Butterworth Heinemann, Burlington, MA, 1989.

Spichtinger, P. and Cziczo, D.J..: Aerosol–cloud interactions—a challenge for measurements and modeling at the cutting edge of cloud–climate interactions, Environ. Res. Lett., 3, 025002, doi:10.1088/1748-9326/3/2/025002, 2008.

Wiedensohler, A. and Birmili, W. and Nowak, A. and Sonntag, A. and Weinhold, K. and Merkel, M. and Wehner, B. and Tuch, T. and Pfeifer, S. and Fiebig, M. and Fjäraa, A. M. and Asmi, E. and Sellegri, K. and Depuy, R. and Venzac, H. and Villani, P. and Laj, P. and Aalto, P. and Ogren, J. A. and Swietlicki, E. and Williams, P. and Roldin, P. and Quincey, P. and Hüglin, C. and Fierz-Schmidhauser, R. and Gysel, M. and Weingartner, E. and Riccobono, F. and Santos, S. and Grüning, C. and Faloon, K. and Beddows, D. and Harrison, R. and Monahan, C. and Jennings, S. G. and O'Dowd, C. D. and Marinoni, A. and Horn, H.-G. and Keck, L. and Jiang, J. and Scheckman, J. and McMurry, P. H. and Deng, Z. and Zhao, C. S. and Moerman, M. and Henz-

ing, B. and de Leeuw, G. and Löschau, G. and Bastian, S.: Mobility particle size spectrometers: harmonization of technical standards and data structure to facilitate high quality long-term observations of atmospheric particle number size distributions, Atmos. Meas. Tech., 5, 657–685, doi:10.5194/amt-5-657-2012, 2012.

Table 1. List of important symbols

Parameter	Notation
General parameters	
SS	supersaturation
SS_{peak}	effective peak supersaturation (Hammer et al., 2014)
SS_{crit}	critical supersaturation (Köhler, 1936)
w	updraft velocity
Measured parameters	
w_{act}^{meas}	measured updraft velocity
Estimated parameters	
SS_{peak}^{estim}	estimated effective peak supersaturation derived from measurements (see Sect
w_{act}^{estim}	estimated updraft velocity derived from measurements and topography (see Sec
Modelled parameters	
SS_{peak}^{mod}	modelled effective peak supersaturation
SS_{peak}^{ref}	effective peak supersaturation obtained from the reference model simulation
SS_{mod}^{max}	maximum relative water vapour pressure between the model initialization point a
w_{act}^{mod}	modelled updraft velocity
w_{mod}^{divX}	modelled updraft velocity divided by X
w_{mod}^{mulX}	modelled updraft velocity multiplied by X
SS_{peak}^{fluc}	modelled effective peak supersaturation applying the real-time fluctuations
$SS_{peak}^{fluc,sin}$	modelled effective peak supersaturation with a sinus function

Table 2. Box model input parameters used for Fig. 3. The 25th, median and 75th percentile of the dry aerosol number size distribution were calculated binwise. The median and 75th percentile of the dry aerosol number size distribution resulted in a bimodal distribution and thus two modes are given.

Measured parameter(s)		25th percentiles	median	75th percentiles
Hygroscopicity parameter [–]		0.19	0.26	0.37
Dry aerosol number	modes [nm]	50	51, 131	46, 136
size distribution	FWHM* [nm]	102	179	200
Temperature at the JFJ [K]		270	272	273
Pressure at the JFJ [hPa]		659.6	660.5	663.2
Total water content [$mg\,m^{-3}$]		4110	4750	5200

* Full width at half maximum.
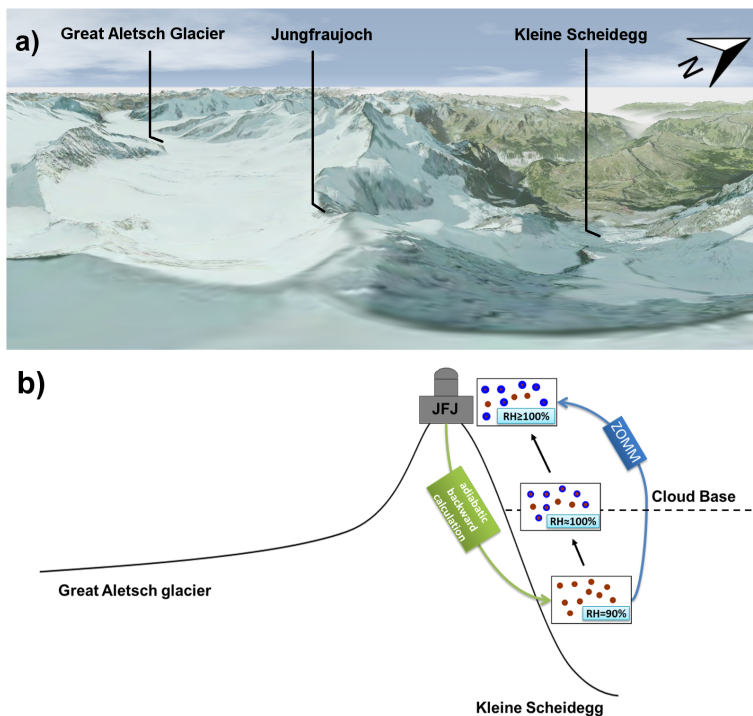
Figure 1. In **(a)** a panorama picture is shown to give an overview of the surrounding of the Jungfraujoch. The topography is shown in a sketch **(b)** along with the subsaturated conditions, conditions at the cloud base and at the Jungfraujoch. The green arrow shows the adiabatic backward calculations for the conditions at subsaturated conditions (initialization point of ZOMM; RH = 90 %) with the measurements performed at the Jungfraujoch. The blue arrow shows the direction from the initialization point of the model until the end state of the simulation, which is at the Jungfraujoch. Brown dots indicate aerosol particles, blue dots cloud droplets.

31
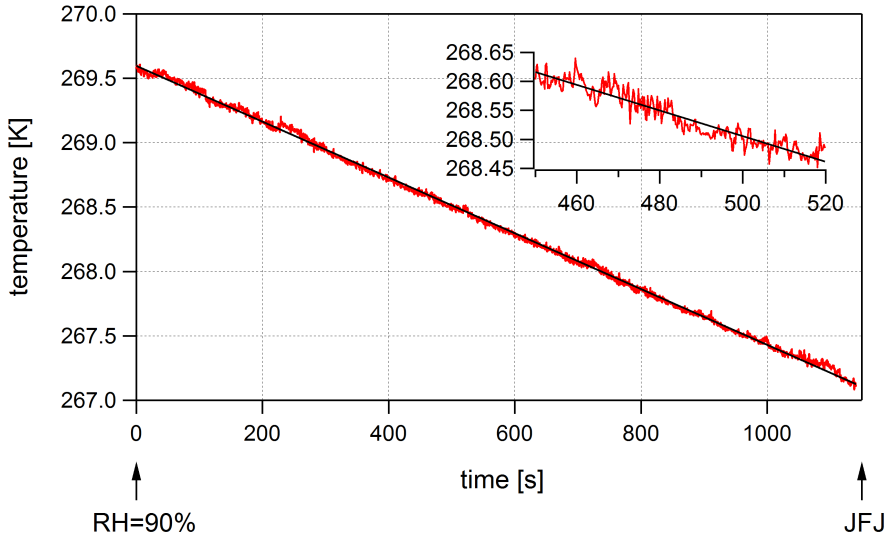
Figure 2. For the model run #516, which was detected on 8 August 2011 18:20 UTC, the temperature trajectory is shown with the added small-scale temperature fluctuation (T_{turb}) retrieved from the sonic anemometer measurements (see detailed description in Sect. 2.3.1). The inset shows the trajectory on a smaller scale for a more quantitative view of the small-scale temperature fluctuations.
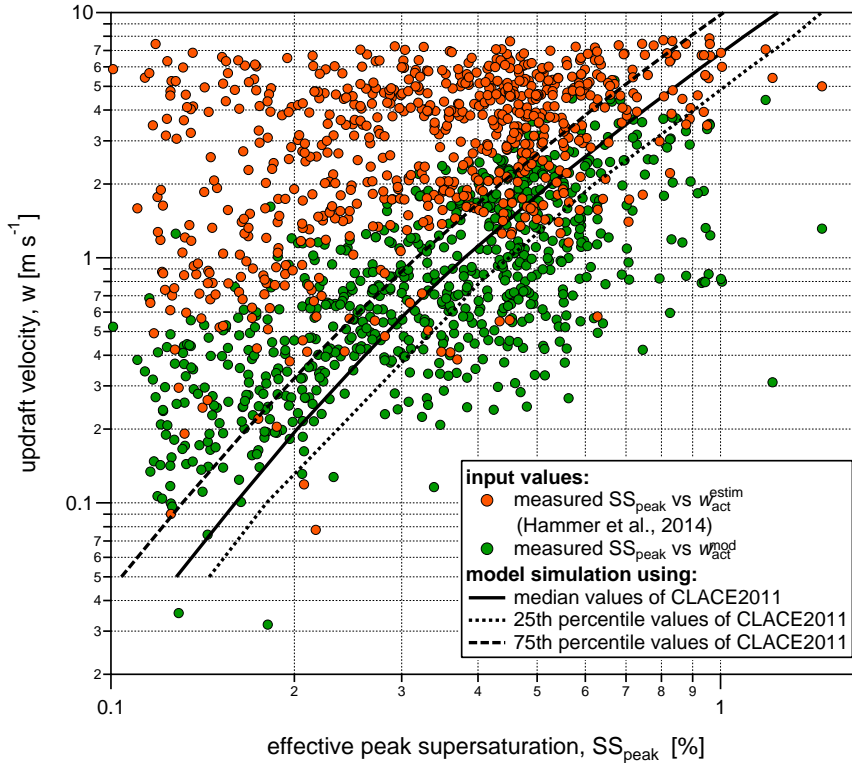
Figure 3. Each circle represents a trajectory calculation while the black lines show the trajectory calculations with the 25th, median and 75th values of the whole campaign given in Table 2. The relationship between the retrieved updraft velocity (w_{act}^{estim}) and effective peak supersaturation (SS_{peak}^{estim}) is given in red circles while the relationship of the simulated updraft velocity at cloud base (w_{act}^{mod}) and SS_{peak}^{estim} is given in green circles.
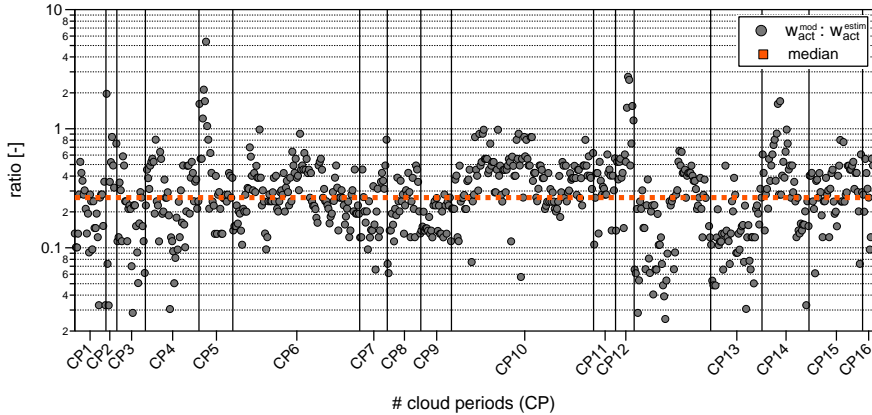
Figure 4. Ratio of the simulated updraft velocity (w_{act}^{mod}) and the estimated updraft velocity at the cloud base (w_{act}^{estim}) for each model simulation categorized for the different cloud periods (CP). The lines and the labels of CP serve to identify different cloud periods between which there are gaps of non-cloudy time. The orange line indicates the median ratio of $w_{act}^{mod} : w_{act}^{estim}$.
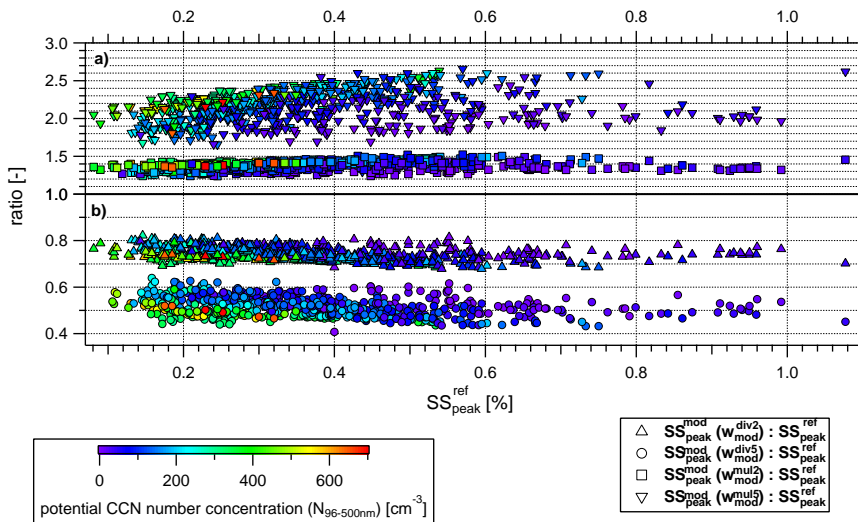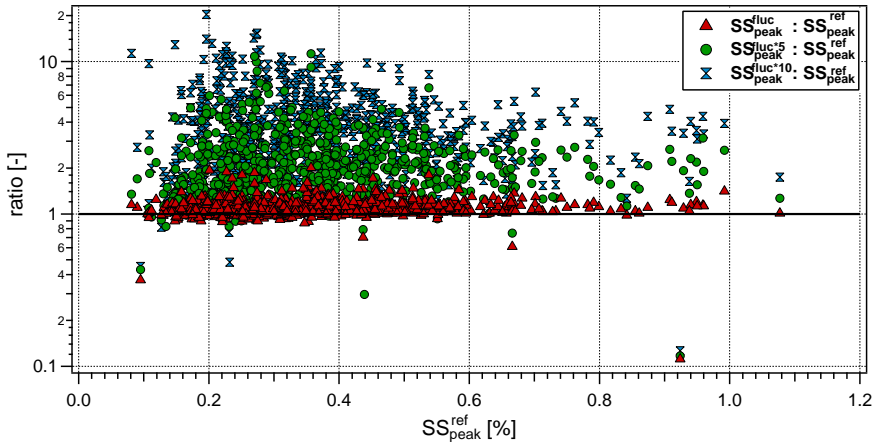
Figure 5. Ratio of modelled effective peak supersaturations using two different data sets of updraft velocities as input parameter: once divided and multiplied by 2 (w_{act}^{div2}, w_{act}^{mul2}) and once divided and multiplied by 5 (w_{act}^{div5}, w_{act}^{mul5}) to the reference updraft velocities (w^{ref}). The points are colour coded to show the number concentration of particles in the size range of 96 nm (median dry activation diameter of CLACE2011) to 500 nm (upper limit of the SMPS). This is considered to be the potential CCN number concentration.
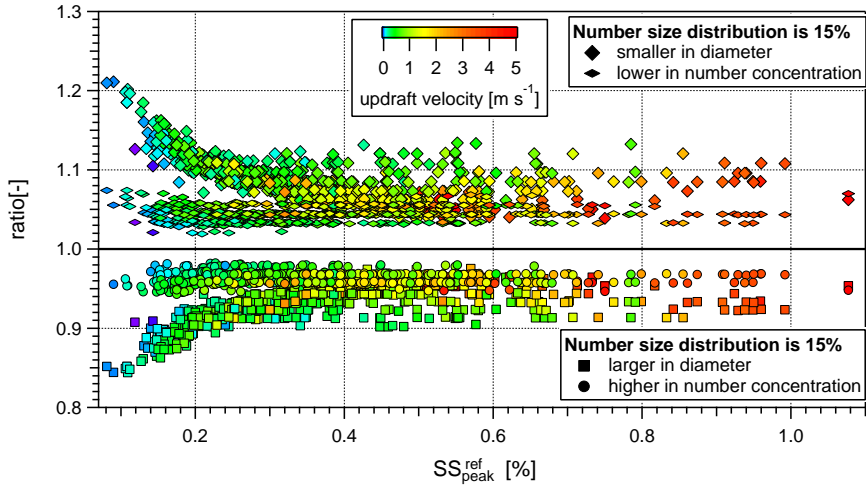
Figure 6. Ratio SS_{peak} : SS_{peak}^{ref} using: 15 % higher (circles) and lower (flat diamonds) particle number concentration compared to the measured one, and 15 % larger (squares) and smaller (diamonds) particles compared to the measured size distribution. All symbols are colour coded to show the modelled updraft velocities.
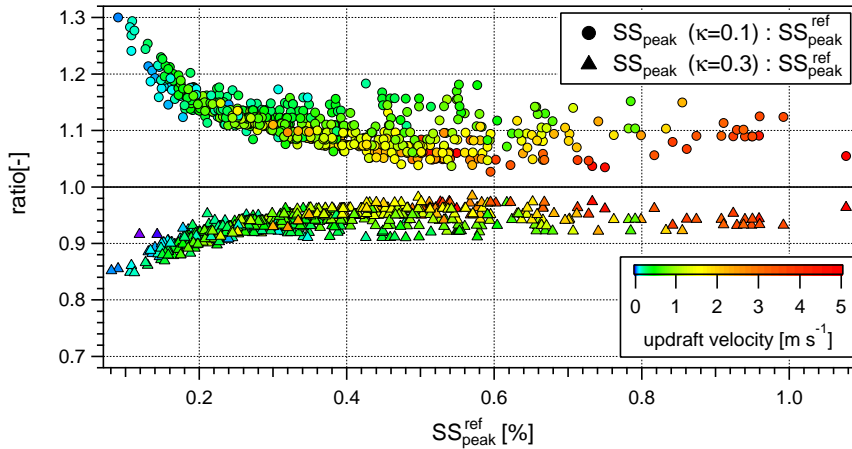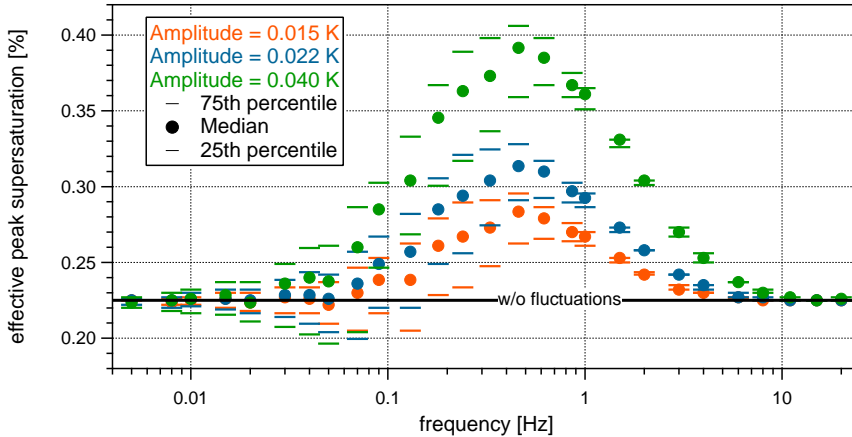
Figure 7. Ratio of effective peak supersaturation values using either a hygroscopicity value $\kappa = 0.1$ and 0.3 to the median hygroscopicity parameter measured at the Jungfraujoch of $\kappa = 0.2$. The points of the datasets are colour coded to show the modelled updraft velocities.

Figure 8. Ratio of modelled effective peak supersaturations applying small-scale fluctuations (obtained from the ultrasonic anemometer measurements) to the cooling rate, to the SS_{peak}^{ref}. The small scale-fluctuations are multiplied by 1 (SS_{peak}^{fluc}; red triangles), 5 ($SS_{peak}^{fluc \cdot 5}$; green triangles), and 10 ($SS_{peak}^{fluc \cdot 10}$; blue triangles).
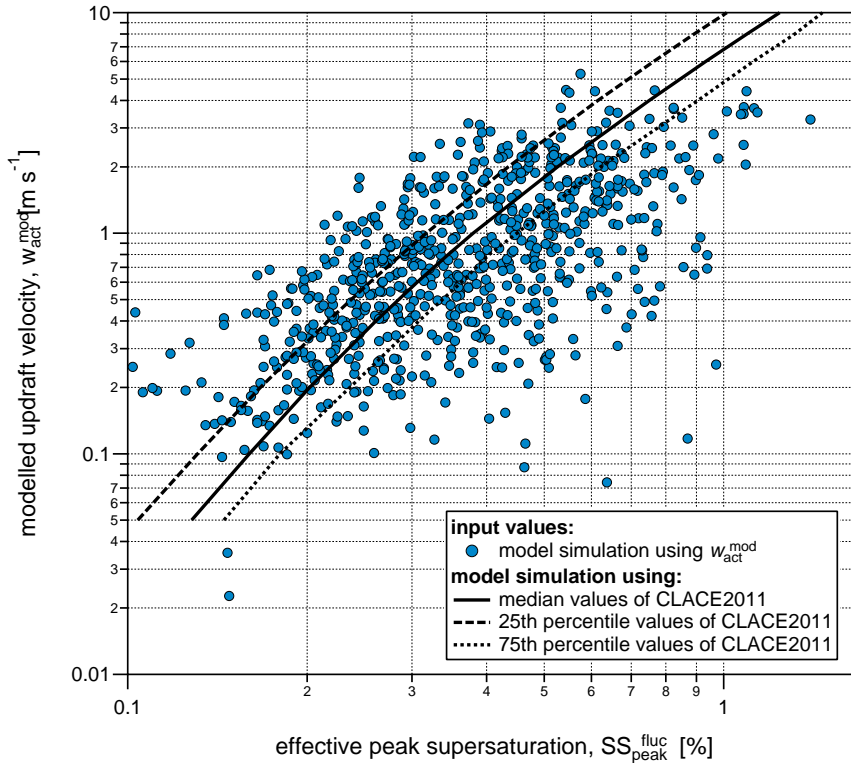
Figure 9. Same as Fig. 3 but the relationship between the modelled updraft velocity (w_{act}^{mod}) and effective peak supersaturation taking into account the small-scale fluctuations (SS_{peak}^{fluc}).
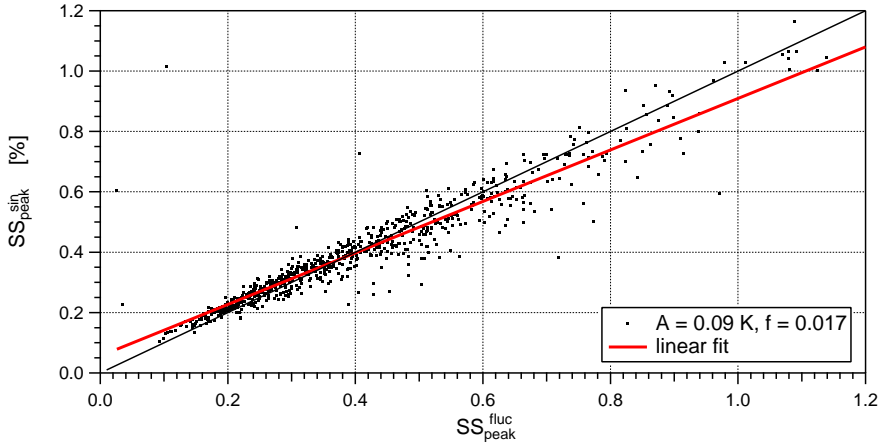
Figure 10. Dependency of the modelled effective peak supersaturations applying simulated small-scale fluctuations ($SS_{peak}^{fluc,sin}$) to the cooling rate on the frequency. The applied small-scale fluctuation were obtained with a sinus function using three different amplitudes $A = 0.015$ (red), 0.022 (blue) and 0.04 K (green), several frequencies in the range from 0.05 to 20 Hz and phases from 0 to 360° with 18° steps. The circles indicate the median values, while the bars show the 25th and 75th percentiles.
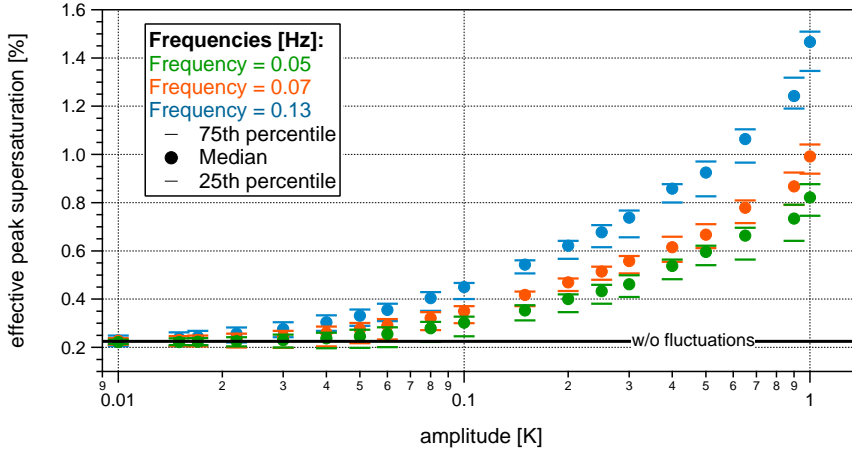
Figure 11. Dependency of the modelled effective peak supersaturations applying simulated small-scale fluctuations ($SS_{peak}^{fluc,sin}$) to the cooling rate on the amplitude. The applied small-scale fluctuation were obtained with a sinus function using three different frequencies $f = 0.05$ (green), 0.07 (red) and 0.13 Hz (blue), several amplitudes in the range from 0.01 to 1.5 K and phases from 0 to 360° with 18° steps. The circles indicate the median values, while the bars show the 25th and 75th percentiles.

Figure 12. Modelled effective peak supersaturations applying simulated small-scale fluctuations ($SS_{peak}^{fluc,sin}$ obtained with a sinus function using an amplitude $A = 0.022$ K and a frequency $f = 0.24\,s^{-1}$) to the cooling rate vs. the one applying small-scale fluctuations obtained from the ultrasonic anemometer measurements (SS_{peak}^{fluc}). The black line indicates the $1:1$ line and the red line shows the linear fit.